Planetary atmospheres minor species sensor balloon flight test to near space

Robert E. Peale*[a], Christopher J. Fredricksen[a], Andrei V. Muraviev[a], Douglas Maukonen[a], Hajrah M. Quddusi[a], Seth Calhoun[a], Joshua E. Colwell[a], Timothy A. Lachenmeier[b], Russell G. Dewey[b], Alan Stern[c], Sebastian Padilla[c], Rolfe Bode[c]

[a]Dept. of Physics, University of Central Florida, 4000 Central Florida Blvd., Orlando, FL USA 32816-8005; [b]Near Space Corporation, 5755 Long Prairie Rd., Tillamook, OR USA 97141-9688; [c]World View Enterprises, Inc. 1840 East Valencia Rd., Tucson, AZ USA 85706-5800.

ABSTRACT

The Planetary Atmospheres Minor Species Sensor (PAMSS) is an intracavity laser absorption spectrometer that uses a mid-infrared quantum cascade laser in an open external cavity for sensing ultra-trace gases with parts-per-billion sensitivity. PAMSS was flown on a balloon by Near Space Corporation from Madras OR to 30 km on 17 July 2014. Based on lessons learned, it was modified and was flown a second time to 32 km by World View Enterprises from Pinal AirPark AZ on 8 March 2015. Successes included continuous operation and survival of software, electronics, optics, and optical alignment during extreme conditions and a rough landing. Operation of PAMSS in the relevant environment of near space has significantly elevated its Technical Readiness Level for trace-gas sensing with potential for planetary and atmospheric science in harsh environments.

Keywords: gas sensor, intracavity laser absorption, quantum cascade laser, high-altitude balloon, near space
*Robert.Peale@ucf.edu; phone 1 407 823-2325; fax 1 407 823-5112; http://www.physics.ucf.edu/~rep/

1. INTRODUCTION

The Planetary Atmospheres Minor Species Sensor (PAMSS) is an intracavity laser absorption spectrometer that uses a mid-IR quantum cascade laser in an open external cavity for sensing ultra-trace gases and vapors. The system comprises integrated laser/optical/spectroscopic and electronics/software units. Atmospheric samples enter the open external laser cavity, where active-cavity gain allows optical path length through the sample to exceed a kilometer due to multiple reflections between cavity mirrors that are separated by centimeters. This potentially gives exponentially higher sensitivity for ultra-trace gas detection than (e.g.) the Tunable Laser Spectrometer on the Mars Curiosity Rover, which recently detected the bio-indicator gas methane.[1] Other potential planetary science applications include search for life on Enceladus and Europa, greenhouse chemistry on Venus, and compositional analysis for exotic atmospheres on Saturn's moon Titan. Earth science applications include detection and analysis of climate changing gases, ozone, acid rain, and air pollution. Terrestrial applications include medical breath tests to diagnose disease and explosives detection for public safety.

Balloon flights to near space for PAMSS were provided by the NASA Flight Opportunities Program. The purpose is instrument maturation, where the entry Technical Readiness Level (TRL) must be 4, i.e. a functional prototype operating in the laboratory. Such was demonstrated for PAMSS,[2] where the system operating principles are described. Additional development achieved a stand-alone instrument capable of operating outside the laboratory on battery power with a total mass under 10 kg suitable as a small balloon payload.[3]

Fig. 1 presents a photograph of PAMSS before the first flight. The upper portion is the optics/laser/spectroscopic component. The lower portion is the electronics component. Data acquisition and control were achieved using a National Instruments compact Realtime I/O (cRIO) system with 8 plug-in modules. The software was developed in Labview and loaded onto the field programmable gate array (FPGA) of the cRIO, which controlled a laser driver, a thermoelectric cooler (TEC), and a scanning Fabry-Perot (FP) interferometer.

Monitored signals include temperatures (QCL, heat-sink, ambient), the voltage applied to the QCL under constant current excitation, and the detector signal. Combined system weight was 9.9 kg including Li batteries. The laser operated at 8.1 μm wavelength and had been calibrated for detection of water vapor at absorption coefficients as low as 1 x 10^{-5} cm^{-1}, which corresponds to 40 ppb.[2]

Critical to the sensitivity of PAMSS is the laser cavity alignment. The beam exits the multi-mode QCL active region, which has a minimum dimension of just 10 μm, via an anti-reflection (AR) coating. The strongly divergent beam is captured and collimated by a fast AR-coated ZnSe lens. A flat gold-coated mirror with a 1 mm hole for output coupling completes the cavity. The return beam must re-enter the 10 μm active region in order to experience the gain that compensates for cavity losses and which gives the long effective path lengths responsible for the potentially unprecedented sensitivity. Very small perturbations can disrupt the feedback and eliminate any sensitivity advantage over passive cavity approaches. The output laser passes through the FP, which acts as a narrow band-pass filter with free spectral range exceeding the laser spectral bandwidth and resolving power (Q) sufficient to resolve pressure-broadened absorption lines in range of the laser. The alignment of the FP is also critical to achieving adequate Q, but this should be less sensitive to perturbations. For the flight, a sensitive room-temperature pyroelectric detector was used, though its response time was known to be too slow to monitor mode dynamics, which were shown in the lab using a 77 K HgCdTe detector to be a sensitive indicator of intracavity absorption.[2]

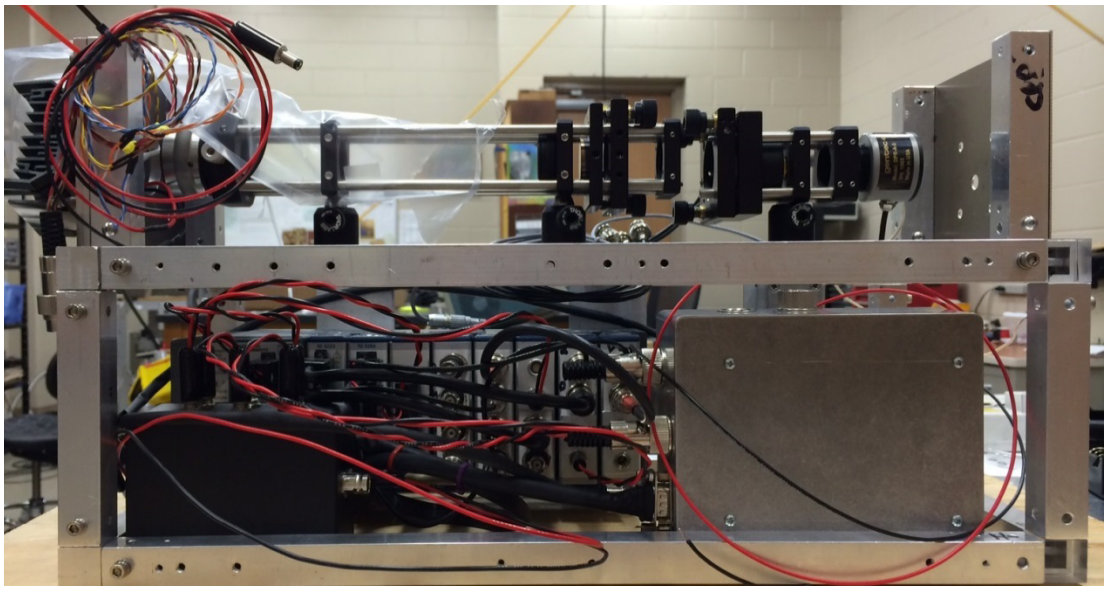

Figure 1. Photograph of PAMSS prior to first flight

Thus, one of the primary objectives of the flight was to monitor the robustness of the laser cavity alignment as the system underwent extreme changes of pressure and temperature combined with accelerations due to launch, winds, handling, and descent by parachute. Indicators of that alignment include the spectra collected, the voltage applied to the laser under constant current excitation, and spikes on that voltage that occur when the laser mode spectrum changes during heating of the active QCL crystal for long pulse (~10 ms) excitation. When alignment is good, the voltage is minimized and the spikes are maximized.

2. FIRST FLIGHT

PAMSS was flown on a balloon by Near Space Corporation from Madras OR to 30 km on 17 July 2014. Flight objectives were to maintain an altitude of 27.4 km for at least 10 minutes, to monitor temperatures of key components, to record data on the status of the laser, the optical alignment, and the status of the electronics, and to collect the spectrum of a weak line of water vapor throughout the flight duration. Fig. 2 presents photographs of the launch. Flight objectives were achieved by maintaining an altitude higher of 30 km for 20 minutes. Successes of the payload operation

included continuous functioning and survival of software, electronics, optics, laser, and optical alignment during the extreme conditions of flight and a hard landing. Anomalies were that data collection on some channels was corrupted. The system pictured in Fig. 1 proved susceptible to electromagnetic interference (EMI) due to its open architecture, absence of shielding, plastic joints on the frame, and long unshielded loops of wire.

Figure 2. Photographs of launch by Near Space Corporation from Madras OR on 17 July 2014.

Unfortunately, no valid data were collected on the laser voltage and detector channels. The suspected cause was that electromagnetic interference from the balloon's telemetry system put those analog inputs into an unusable state, such that every recorded value was "not a number". Such an error had never been observed in three years of laboratory operation without a broadcasting rf antenna nearby. Fig. 3(left) presents a photograph of the balloon gondola, which contains the PAMSS system. The most likely source of electromagnetic interference (EMI) is the downward pointing VHF antenna operating at 138.75 MHz with 1 W power. The GPS Iridium patch antenna mounted at the center of the gondola top plate and operating at 1616-1626 MHz with 7 W should not have caused interference. The VHS antenna radiated upward through the plywood gondola floor and into the unshielded cage of the PAMSS electronics.

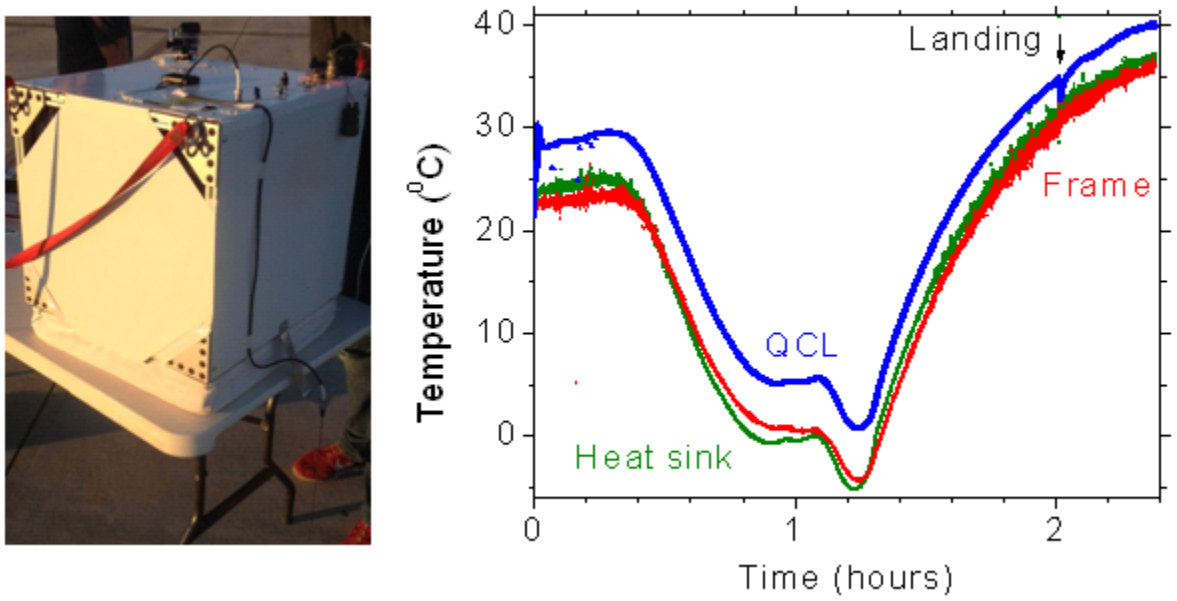

Figure 3. (left) Gondola before 17 July 2014 flight. The VHF antenna points down below the bottom of the gondola. The Dual GPS Iridium antenna is the small black box at center of the aluminum top plate, which should shield the interior of the gondola from this radiation. (right) PAMMS temperature sensor data.

In contrast to the laser voltage and intensity data, useful temperature data were successfully collected by the system, validating proper function of the electronics and software. We had been unsure whether the absence of convective cooling would cause the QCL to require more cooling than what was needed in the lab to maintain the ideal operating temperature of 18 C, or whether radiation into a cold environment would be so effective as to require that heat be applied to the QCL. The temperature data plotted in Fig. 3 (right) from the flight showed that the laser would over-cool at altitude rather than overheat. A spike in the temperature data just after 2 hours indicates the moment of landing. Temperature data continue to be recorded after the rough landing, which ended with the gondola coming to rest upside down. The temperature of the Cu-block on the frame finally reaches the ~35 C ambient temperature of the Oregon desert in the middle of the day in July. The QCL continues to be electrically heated up to 40 C until the payload was recovered and turned off. The TEC was not functioning because its dedicated batteries had died. Positive outcomes were that the laser itself, its anti-reflection coating, and the optical alignment all survived the flight, the hard landing, de-integration, and travel back to Orlando. Inspection under the microscope showed no change in the appearance of the coating.

3. SECOND FLIGHT

Based on the experience of the first flight, and following a decision by the NASA Flight Opportunities Program (FOP) to recycle the payload for a second flight, effort was made to electrically shield the electronics from rf interference. Plastic joints in the aluminum frame were replaced by aluminum joints, so that the entire cage would be at ground potential. The optics system was de-integrated and remounted on a dedicated aluminum plate, so that the optics and electronics could be more easily separated without endangering the optical alignment. Then, sheet aluminum covers were fabricated to cover each face of the electronics cage. A front panel with coaxial bulkhead connectors was fabricated, to allow communication between the optical and electronic systems. Where possible, cables between various subsections within the electronics enclosure were also replaced by coax. Wires were everywhere shortened as much as possible. Batteries were enclosed in a separate shielded box outside of the electronics cage, and power was feed into the cage via coaxial cables and bulkhead connectors. A photograph of the modified PAMSS system is presented in Fig. 4.

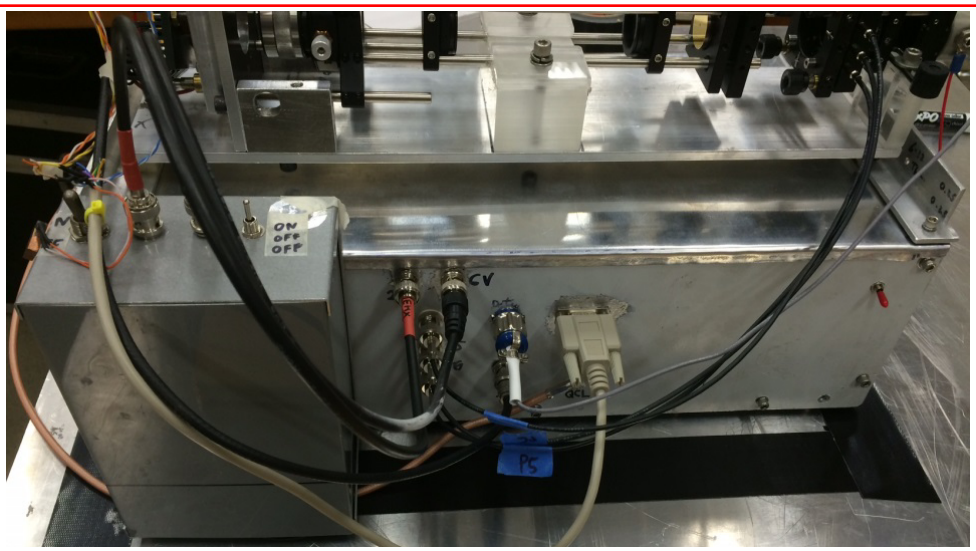

Figure 4. PAMSS after shielding

NASA FOP chose World View Enterprises (WV) to provide the second balloon flight. Fig. 5 presents photographs of the launch on 8 March 2015 from Pinal Airpark AZ. In addition to lifting our now 11 kg payload (after shielding), the WV Stratocraft contained a cosmic ray experiment from Gannon University (16 kg).

Figure 5. Launch and flight by World View Enterprises from Pinal Airpark AZ on 8 March 2015. Photo credits (left) J. Martin Harris Photography and (right) Gregory Claxton

Fig. 6 (left) presents altitude, pressure, and temperature data provided by World View (WV). Before launch a stable elevation value of 0.575 km is recorded, which is in agreement within 2 m of the 0.577 km altitude of the Pinal Airpark AZ launch site. According to the altitude data, the launch occurs at 07:06:50 a.m. MST. A float altitude of 32.12 km is achieved at 08:55:26 MST. The apparent ascent duration is 1:48:36 = 1.81 hours. The float duration is 1:37:05 = 1.62 hours. The descent begins at 10:32:31 MST.

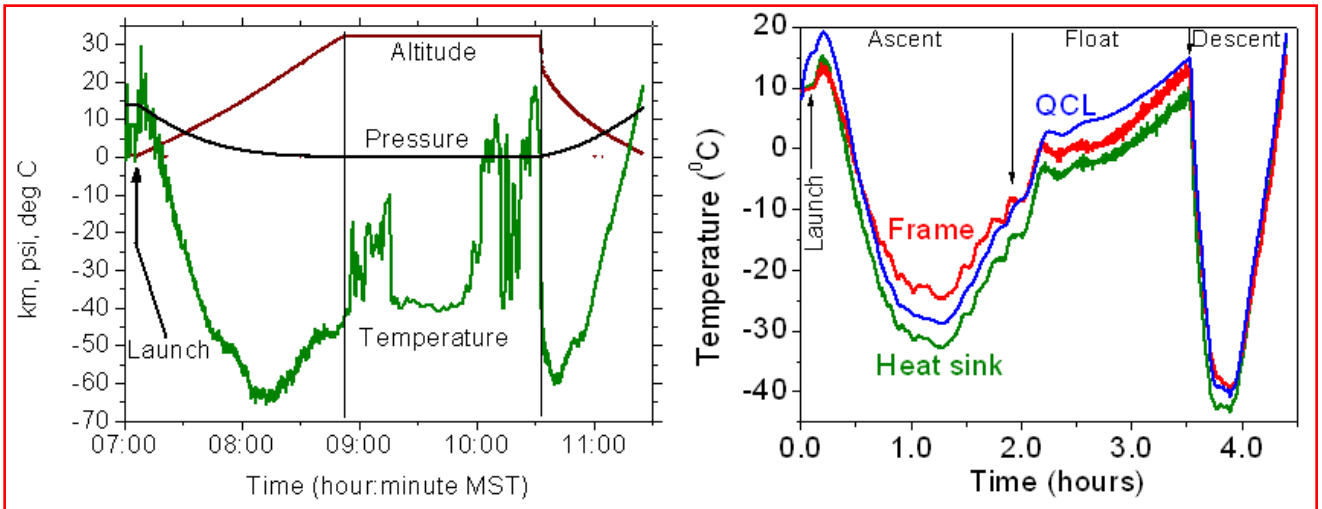

Figure 6. (left) WV flight data. (right) UCF temperature data

The WV temperature data at float shows large excursions from a baseline of -40 C to as high as 20 C. This is reported to be typical and is assumed to be caused by the Stratocraft turning. Sometimes the sensor is in shadow and sometimes it is in direct sunlight. At that altitude, it is very difficult to measure the air temperature, since it is so thin and the metal probe is radiating into space. The radiosonde temperature sensor is a junction hanging in mid-air, which is only recording the temperature of the junction, not really the temperature of the air. Notice that the temperature swings begin just at the start of float and end right after float. During float there is minimal convection. Heat transfer to the sensor junction is dominated by convection during ascent and descent and radiation during float. Isolated outliers also occur, and these are attributed to the transponder and can be ignored.

Fig. 6 (right) presents temperature data recorded by the three temperature sensors on the PAMSS payload. A "QCL" sensor is embedded in a copper block to which the brass QCL mount is attached, and this block does not have direct line-of-sight access to the ambient, though the ambient atmosphere freely flows over it. A "heat sink" sensor is attached to a second copper block between a radiator and a thermoelectric cooler, which is attached to the QCL block. The radiator is exposed to space. A "Frame" sensor is embedded in a third copper block, which is attached to a corner of the aluminum frame, and this sensor has line of sight exposure to the ambient. The WV altitude data has been used to identify the moments of launch, reaching the float altitude, and beginning of descent. The QCL temperature only briefly reached the 18 C temperature that requires the TEC to be activated. Thus, we obtained no information on the performance of the TEC. (Heating function by the TEC had not been implemented by the time of the flight.) Immediately after the launch the QCL temperature began to rise rapidly, in agreement with the WV temperature data, presumably as the payload passes through air that had been heated longer by the rising sun. Then temperatures drop as the payload enters colder air at higher altitude. At the lowest ambient temperature, the QCL is curiously colder than the frame, which may be exposed to the sun, though Joule heating occurs in the QCL. The heat sink is always colder than the QCL, which is expected since the TEC is not operating. There are slow oscillations in all temperatures until float is achieved. In comparison with the WV temperature data, the PAMSS temperatures do not show wild fluctuations, because the sensors are imbedded in Cu blocks with significant thermal mass.

Temperatures rise steadily to ~15 C by the end of the float, which indicates that at this altitude radiative cooling is insufficient, so that the QCL would exceed its optimum 18 C operating temperature eventually. Then it would need to be cooled. This new and important information is owed to the longer duration of the second flight. Without this, we might have been tempted to eliminate the TEC and replace it with a simple resistive heater. Now we know that *both* heating and cooling capability are essential. Because the frame temperature also rises, in fact faster than the QCL, the temperature rise is not primarily due to the Joule heating of the QCL, since the frame and QCL are well separated thermally. The temperature is primarily controlled by the environment and probably solar heating.

A key performance criterion is the maintenance of optical alignment, as indicated by the voltage across the QCL for constant current excitation. After passing through the open section of the laser cavity, the beam must re-enter the QCL's active region, whose dimension is only 10 micrometers. The cavity was aligned before the launch, and the signatures of

alignment are a minimum in laser voltage and maximum amplitude of spikes due to mode-hops on the QCL voltage transient, as shown in Fig. 7 (right). Fig. 7 (left) presents a plot of the laser voltage as a function of time throughout the flight. By comparison with Fig. 6, the QCL voltage changes opposite to the QCL temperature. When the QCL gets cold, the voltage rises. This could be interpreted as a decrease in QCL impedance with decrease in temperature, which can be due to thermal expansion that changes inter-quantum-well tunneling rates. Or, it could indicate a reversible loss of alignment as the temperature drops. Note that the minimum voltages (as occurs for best alignment) occur at the warmest temperatures, which are close to the room temperature at which the cavity alignment was performed. Which of the two possible mechanisms is responsible can be determined by future environmental chamber experiments in the lab.[3]

An important point is that the final QCL voltage is about the same as the initial voltage. However, the final temperature (~18C) is closer to the temperature at which alignment was performed than was the initial temperature (~10 C), so the final QCL voltage should be lower than its initial value if the alignment was well preserved during flight. This suggests that the large swings in temperature may have caused a permanent partial loss of alignment, although complementary evidence based on voltage spikes and discussed below suggests that the alignment was well preserved.

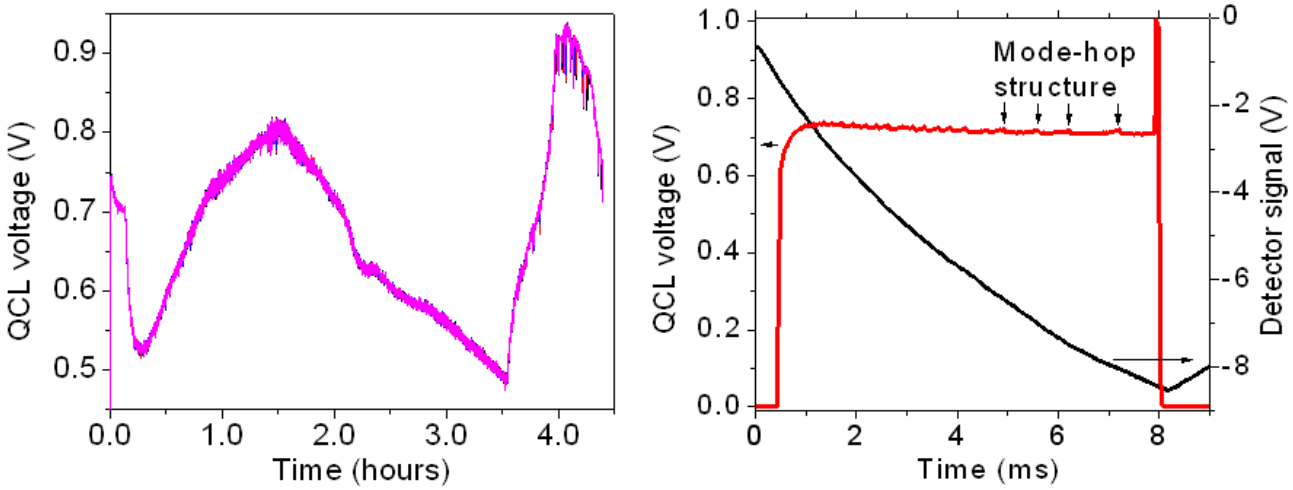

Figure 7. (left) QCL voltage as a function of time. (right) Detector signal and QCL voltage as a function of time for a single laser pulse before the launch.

Fig. 7 (right) explains the nature of the QCL voltage and detector signal. These transients were collected just before the launch. The laser voltage shows a fine structure of spikes due to mode hops that indicate good alignment and feedback for the external cavity. Detector signal is increasingly negative with increasing incident intensity. The rise time of the room temperature pyroelectric detector used for this test is comparable to the 8 ms pulse duration.

Fig. 8 shows the spikes on the QCL voltage at the beginning and at the end of the flight. These spikes only appear when there is good alignment and feedback into the active region of the QCL. That the spike amplitudes are very similar in both traces indicates that there was no significant permanent loss of alignment during the flight.

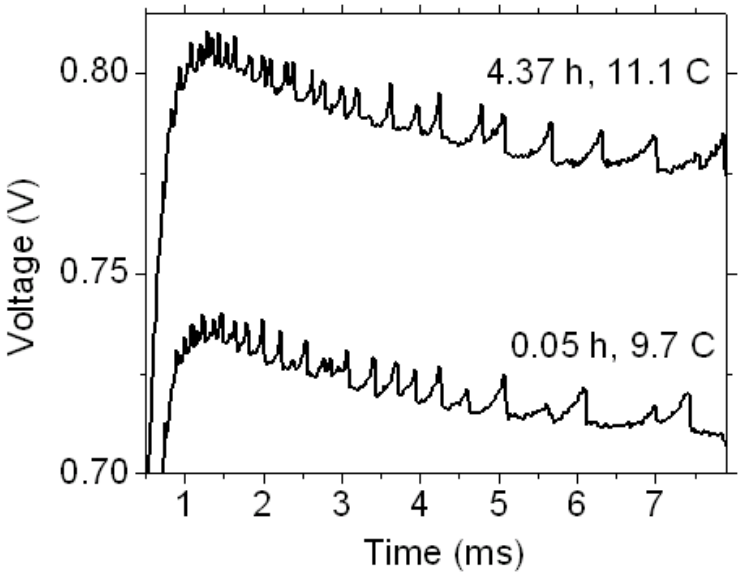

Figure 8. QCL voltage transients showing spikes due to mode hops. The spikes are diagnostic of good alignment.

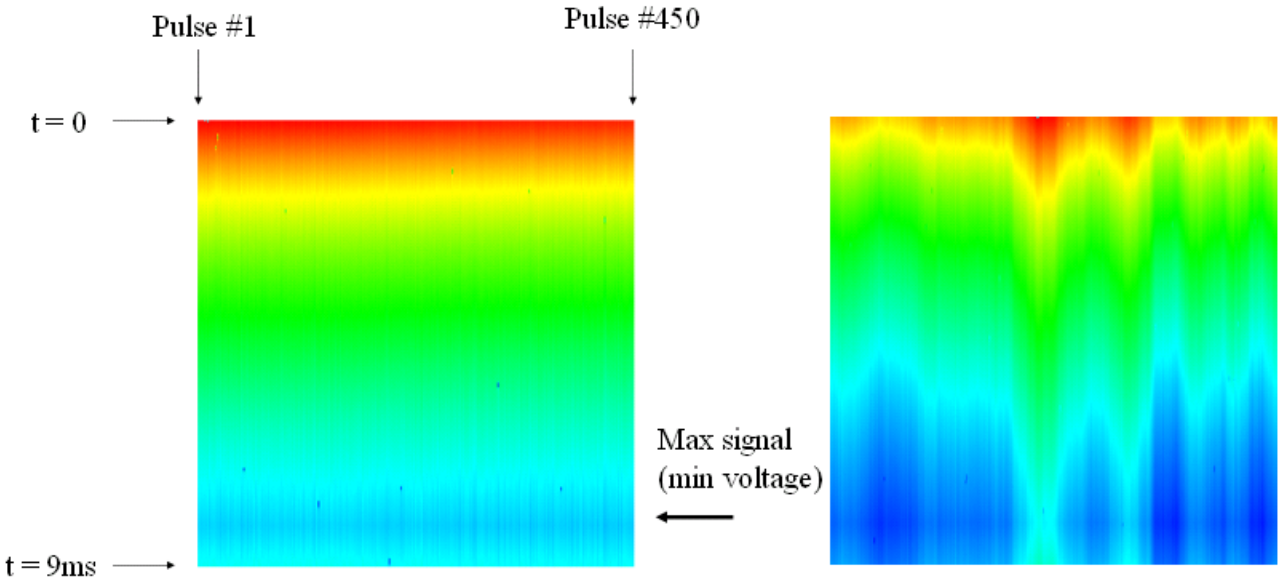

Figure 9. Laser intensity (color) vs time and pulse number. Each pulse has a successively larger Fabry-Perot etalon spacing. Color indicates intensity with red (near the top) being the lowest and blue (near the bottom) the highest.

Fig. 9 presents examples of the time dependent spectral data. During the flight, 316 such spectra were collected. When all pulses go from red to blue uniformly across the image, as in Fig. 9 (left), they are going from roughly the same starting voltage to the same ending voltage. The next spectrum would be scaled individually, so it may look the same but have different voltage endpoints (instead of -0.75V to -8.25V, it may be -1V to -9V, etc.), due to a baseline shift that we attribute to a change in background temperature.

Fig. 9 (right) presents an example spectrum collected immediately after the launch. Preliminary interpretation of the variations observed with FP spacing is that they are artifacts due to temperature variations caused by gusting winds. The wind blows cold air across the face of the detector causing an artificial decrease in the signal. Such might be mistaken as a molecular absorption line, except that they are different from spectrum to spectrum.

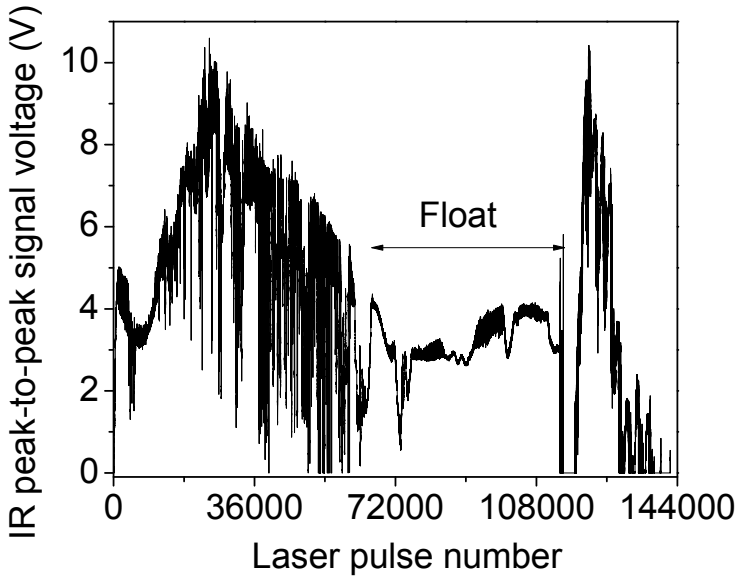

Fig. 10. Peak-to-peak detector signal vs. laser pulse number.

Fig. 10 presents a plot of peak-to-peak laser signal, namely I(0 ms) – I(8 ms) for each pulse, as a function of laser pulse number. Every 450 pulses corresponds to one complete sweep of the Fabry-Perot. Each sweep is separated by 2-3 seconds. The total is 316 FP sweeps. The total number of laser pulses was 450 x 316 = 142200. The signal strength varies throughout the flight, punctuated by many-downward excursions toward zero. Inspecting the signal transients at those points shows that they occur due to a baseline shift toward either positive or negative rail. When the baseline is saturated at a rail, the peak-to-peak signal voltage is naturally zero. The signal is relatively stable and unsaturated during float, but as soon as the Stratocraft was dropped, the signal saturated at the positive rail. We interpret this as a relatively warm detector, which had been heated during float as shown in the temperature data, suddenly seeing a colder background at lower elevations. As the Stratocraft approached the ground, the signal saturated at the negative rail, which we interpret as the now relatively cold detector seeing a warm background at lower elevations. The lesson learned is that the detector should be restricted to see only laser light, using as minimum a baffle that is in thermal equilibrium with the detector to limit the field of view, and a narrow band pass filter to admit only the laser wavelength. The detector may also need to be temperature stabilized.

When the Stratocraft landed, data acquisition was aborted, but evidence showed that the system tried to reboot itself. The laser may have operated on the ground for the hour it took to locate and recover the payload, but no data was recorded. Back in Orlando, we discovered that the laser no longer functioned, though laser signal was recorded right up to landing. Inspection under the optical microscope (Fig. 11) showed that the laser facet was burned. This may have been caused by contamination at the facet, due either to dust kicked up by the landing, or by moisture condensing on the cold crystal, which would cause absorption of laser power at the level of 10 MW/m^2 with consequent local damage caused by heating. We have had previous experience of AR-coated QCLs being destroyed in this way. The lesson learned is that the laser must be protected from environmental contamination. This argues against the passive introduction of ambient vapors into an open cavity. Instead filtered and dried air should be drawn into the cavity in such a way that the gas or gases of interest are not also removed. The potential for catastrophic damage (and sensitivity to misalignment) would be lessened by using ring-cavity surface emitting QCLs, which have much larger exit apertures, should these become commercially available.

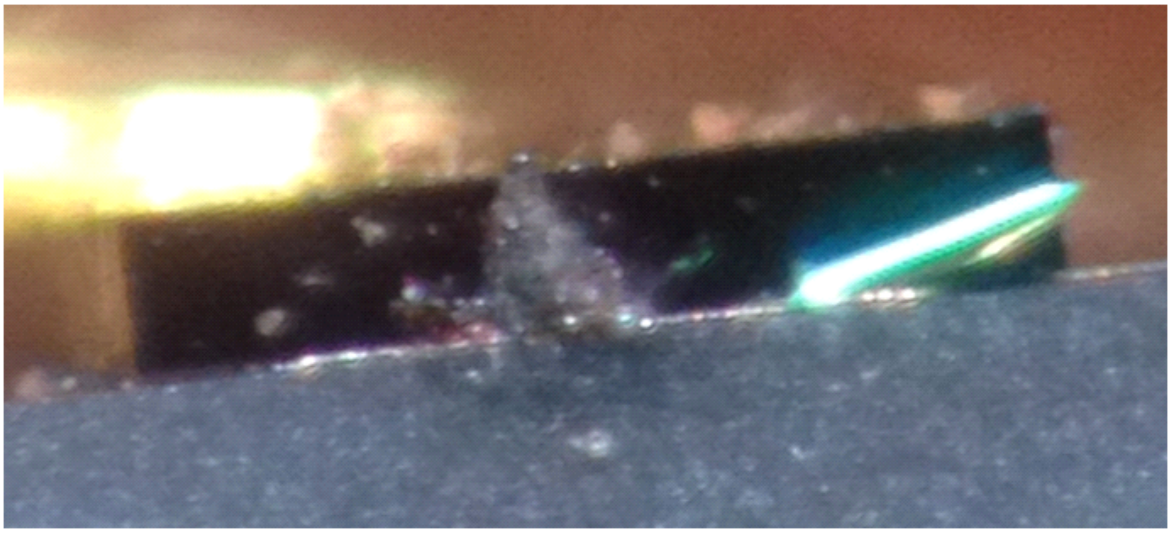

Fig. 11. Burned end facet of QCL. The bright stripe on the right lower corner of the laser is a partial peeling of the anti-reflection coating that was present before the first flight.

In summary, the PAMSS instrument successfully acquired data during the second balloon with expected characteristics. Wind-induced artifacts were observed in the spectra. Important lessons learned are that temperature control with both heating and cooling capability needs to be implemented, the optical path should be shielded from wind, and dynamic alignment to compensate for the possibility of thermal distortion of the laser cavity should be implemented. The detector should be shielded and filtered from background radiation that affects the signal baseline. The QCL must be protected from environmental contamination. A more stable cavity configuration based on semi-confocal design with a single spherical mirror should be also considered.

ACKNOWLEDGEMENTS

The balloon flights were funded by the NASA Flight Opportunities Program. Support for UCF personnel was provided by the Florida Space Institute and the Center for Microgravity Research.

REFERENCES

[1] Webster, C. R., et al. “Mars methane detection and variability at Gale crater,” Science 347(6220) 415-417 (2015).
[2] Muraviev, A. V., Maukonen, D. E., Fredricksen, C. J., Gautam Medhi, and Peale, R. E., “Quantum cascade laser intracavity absorption spectrometer for trace gas sensing,” Appl. Phys. Lett. 103(9), 091111 (2013).
[3] Maukonen, D., Fredricksen, C. J., Muraviev, A. V., Alhasan, A., Calhoun, S., Zummo, G., Peale, R. E., Colwell, J. E., “Planetary Atmospheres Minor Species Sensor (PAMSS),” Proc. SPIE 9113, 91130N (2014).